Acta Biochim Biophys Sin xxxx, xx(x): xx-xx
https://cstr.cn/32197.14.abbs.2026035
https://doi.org/10.3724/abbs.2026035
Original Article

Original Article

Scaffold compound T4015 attenuates pulmonary fibrosis via suppressing JAK/STAT and NF-κB signaling

Minghui Zhang[1,†], Hang Xu[1,†], Shan Liu[2,†], Xiaohan Xu[1,†], Jiayi Yin[1], Xinxin Zhang[2], Xiaonan Zhang[2], Xiaoping Yang[3,4], Xiaochun Liu[2], Bin Yin[3], Mingming Zhou[2], Lewei Wang[1], Meng Zhang[1], Huiying Liu[3], Wenqing Jiang[3,*], Qiaoling Song[1,*], and Jinbo Yang[1,*]

[1]Key Laboratory of Marine Drugs, Ministry of Education of China, School of Medicine and Pharmacy, Ocean University of China, Qingdao 266003, China, [2]Marine Biomedical Research Institute of Qingdao, Qingdao 266071, China, [3]Department of Respiratory Diseases, Qingdao Hiser Hospital Affiliated of Qingdao University, Qingdao 266033, China, and [4]First Clinical Medical college, Shandong University of Traditional Chinese Medicine, Jinan 250355, China

[†]These authors contributed equally to this work.

*Correspondence address. E-mail: jiangwenqing126@126.com (W.J.); happysong2023@ouc.edu.cn (Q.S.); yangjb@ouc.edu.cn (J.Y.)

Received 16 August 2025 Accepted 21 November 2025 Published 23 April 2026

Abstract

Pulmonary fibrosis (PF) is a life-threatening interstitial lung disease characterized by scarring and inflammation in lung tissues. Aberrant activation of the JAK/STAT and NF-κB signaling pathways is critical in initiating and sustaining the inflammatory processes that drive fibrotic progression. In this study, we identify a novel small-molecule compound, T4015, a 4-indolyl-2-phenylaminopyrimidine derivative, as a dual-pathway inhibitor targeting both JAK/STAT and NF-κB signaling. Dual-luciferase reporter assays demonstrate the potent inhibitory activity of T4015 against these pathways. T4015 effectively suppresses the phosphorylation of STAT3, JAK1, and TYK2 induced by IL-6 and IFN-β, while suppressing LPS-induced NF-κB activation in macrophages. Transcriptome sequencing and pathway enrichment analyses further confirm that T4015 downregulates multiple inflammation-related signaling cascades, including the JAK/STAT, NF-κB, TNF, IL-17, and Toll-like receptor pathways. In a mouse model of bleomycin-induced PF, T4015 treatment significantly improves survival, attenuates collagen deposition, and reduces the expression of pro-inflammatory and profibrotic markers such as IL-6, CCL2, and COL1. Molecular docking and target prediction analyses suggest that T4015 exhibits strong binding affinity for multiple kinases within the JAK/STAT and NF-κB networks, including JAK1, TYK2, JAK2, JAK3, RIPK1, IRAK1/4, TAB1, and ZAP70. Collectively, these results highlight T4015 as a promising therapeutic candidate for PF through its simultaneous inhibition of the JAK/STAT and NF-κB signaling pathways.

Key words pulmonary fibrosis, JAK/STAT pathway, NF-κB signaling, dual-target inhibitor, inflammation

Introduction

Pulmonary fibrosis (PF) is a chronic interstitial lung disease marked by scar formation and a decline in lung function [1]. Chronic inflammatory diseases are particularly susceptible to progressing into fibrosis, characterized by excessive inflammatory responses and cytokine release [2]. When the cause of PF is unknown, it is referred to as idiopathic pulmonary fibrosis (IPF) [3]. Currently, only two drugs have been approved for the treatment of IPF: pirfenidone, which modulates inflammatory cytokines, and nintedanib, which inhibits tyrosine kinases involved in fibrogenesis [4–6]. However, both drugs show limited efficacy, are associated with adverse effects, particularly hepatotoxicity, and do not improve overall survival [3]. Therefore, the search for safe and effective therapeutic drugs for PF has become an urgent issue in clinical management.

The Janus kinase (JAK)/signal transduction and transcription activator (STAT) pathway is involved in processes such as inflammation, immune response, cell proliferation, and fibrosis [7,8]. Upon cytokine binding, JAKs become activated via autophosphorylation, which subsequently results in STAT phosphorylation and dimerization, driving the transcription of pro-inflammatory and

© The Author(s) 2026. This is an open access article distributed under the terms of the Creative Commons Attribution-NonCommercial-NoDerivs License (https://creativecommons.org/licenses/by-nc-nd/4.0/).

fibrogenic genes [9]. Currently available JAK inhibitors are mainly used to treat autoimmune diseases such as rheumatoid arthritis and ulcerative colitis [10,11]. Growing evidence suggests that the JAK/STAT signaling pathway is involved in the pathogenesis of fibrosis across multiple organs, including the lungs [8]. Notably, interleukin 6 (IL-6)-induced activation of STAT3 has been demonstrated to drive the differentiation of lung fibroblasts into myofibroblasts [10,11]. Furthermore, in patients with IPF, p-STAT3 is highly expressed in lung tissues, primarily located in alveolar macrophages, alveolar epithelial cells, and fibroblasts [10].

Similarly, the nuclear factor kappa-B (NF-κB) transcription factor is instrumental in inducing the expression of pro-inflammatory genes and facilitating the synthesis of cytokines, chemokines, adhesion molecules, and growth factors [12,13]. In the NF-κB signaling pathway, cytokine stimulation triggers the phosphorylation of IκB kinase (IKK), which in turn phosphorylates IκB proteins that are bound to NF-κB. Phosphorylated IκB is subsequently degraded by proteasomes, releasing NF-κB into the cell nucleus to regulate gene expression [14,15]. NF-κB has been extensively studied in various lung diseases characterized by significant inflammatory components, including severe sepsis, acute lung injury, acute respiratory distress syndrome, and cystic fibrosis [16]. It demonstrates marked upregulation during the initial phase of PF [17] and exhibits a strong pathogenic association with multiple pulmonary disorders, including occupational lung diseases and acute lung injury [18]. Importantly, studies have demonstrated that inhibition of the NF-κB signaling pathway can exert therapeutic effects against PF [19].

Importantly, the JAK/STAT and NF-κB pathways are not independent. They share upstream regulators and downstream targets and engage in mutual cross-activation and feedback loops [13,15,19–21]. This crosstalk exacerbates inflammatory signaling, contributing to the chronic immune activation and fibroblast recruitment observed in fibrotic lungs [22–24]. Dual targeting of the JAK/STAT and NF-κB pathways may represent a novel and potentially synergistic therapeutic approach for inflammatory disorders, particularly PF.

In the present study, we employed a high-throughput dual-luciferase reporter screening platform [25] to identify compounds with dual inhibitory activity against JAK/STAT and NF-κB signaling. We identified T4015, a novel 4-indolyl-2-phenylaminopyrimidine derivative, as a potent dual-pathway inhibitor. T4015 effectively suppressed IL-6-induced STAT3 phosphorylation, IFN-β-induced JAK1/TYK2 activation, and lipopolysaccharide (LPS)-induced p-IKK activation in macrophages. Transcriptomic analysis further confirmed broad suppression of inflammatory gene expression, with pathway enrichment pointing to JAK/STAT and NF-κB as the primary affected pathways. *In vivo*, T4015 significantly attenuated PF in a bleomycin-induced mouse model, reducing the expression of *Il6*, *Ccl2*, and collagen I (COL1) and improving lung histopathology. Target fishing and molecular docking suggested its high binding affinity to multiple kinases within both pathways. Collectively, these results demonstrate that T4015, as a promising dual inhibitor of JAK/STAT and NF-κB signaling, possesses potent anti-inflammatory and anti-fibrotic activities and holds considerable therapeutic potential for PF.

Materials and Methods

Experimental reagents

The primary antibodies are listed in Supplementary Table S1. Cell lysis buffer (9803) was purchased from Cell Signaling Technology (Danvers, USA). Recombinant mouse IFN-β protein (12400-1), IL-6 protein (216-16), and IFN-γ protein (315-05) were obtained from PeproTech (Cranbury, USA), and LPS (916374) was purchased from Sigma (Burlington, USA). All scaffold compound and chemical libraries were obtained from TargetMol (Boston, USA).

Luciferase reporter assay

The construction method of the JAK/STAT and NF-κB dual target luciferase reporter system SKA-II was reported in detail in our previous study [25]. SKA-II cells (8000 cells/well) were seeded into white 96-well plates in RPMI 1640 medium and incubated overnight at 37°C in a 5% CO_2 incubator. The following day, cells were exposed to vehicle control or test compounds at the indicated concentrations for 24 h. For high-throughput screening for dual-pathway inhibitors, the prepared compound stock solutions were precisely transferred to 96-well plates with seeded SKA-II cells using a pin tool, with the final concentration of each compound set at 20 μM. Luciferase activity was measured using luciferase kits (E2510; Promega, Madison, USA) and quantified with a SpectraMax® L microplate reader (Molecular Device, San Jose, USA).

Activity screening of structural analogs

To evaluate the inhibitory potency of structural analogs, the compounds were tested at two final concentrations (5 μM and 10 μM), alongside a vehicle control (DMSO; $n = 3$). The compound administration was performed via conventional pipette dosing, and other experimental procedures were the same as the luciferase reporter assay. Relative luciferase activity was calculated by normalizing to the vehicle control, and this normalized value was used to assess inhibitory potency (lower relative activity indicates stronger inhibition).

Western blot analysis

Primary peritoneal macrophages were treated with T4015 (TargetMol) at concentrations of 0, 2.5, 5, 10, and 15 μM for 2 h, followed by stimulation with cytokines (20 ng/mL IL-6, 50 ng/mL IFN-β, 50 ng/mL IFN-γ, or 20 ng/mL TNFα for 10 min) or LPS (100 ng/mL for 30 min) [25,26]. Primary peritoneal macrophages were treated with 10 μM T4015, Tofacitinib (T6321; Topscience, Shanghai, China) [27] and BAY-11-7082 (T1902; Topscience) [28], followed by stimulation with 100 ng/mL LPS for 30min. After stimulation, the cells were washed with ice-cold PBS and lysed in cell protein lysis buffer. Lysate supernatants containing 30 μg protein were separated by SDS-PAGE electrophoresis and transferred onto nitrocellulose membranes (10600034; GE Healthcare, Chicago, USA). After blocking with a 5% nonfat milk solution in TBST (10 mM Tris, pH 8.0, 150 mM NaCl, and 0.1% Tween 20) for 1.5 h, the membranes were incubated with primary antibodies overnight at 4°C. Following washing with TBST three times, the membranes were incubated with HRPconjugated secondary antibodies (Goat anti-Rabbit IgG-HRP Antibody, Abs20002; Absin, Shanghai, China) for 2 h at room temperature. Immunoreactive bands were visualized using Immobilon™ Western Chemiluminescence HRP Substrate (WBKLS0500; Millipore, Burlington, USA) and imaged with a Tanon 5200 imaging system (Tanon, Shanghai, China).

Real-time PCR analysis

Total RNA was isolated from cultured cells or mouse tissues using

RNAiso Plus (9109; TaKaRa, Kusatsu, Japan). Genomic DNA removal and reverse transcription were performed with the PrimeScript™ RT reagent Kit (RR037A; Roche, Basel, Switzerland). Quantitative PCR was conducted on a StepOne Plus Real-Time PCR System (Applied Biosystems, Foster City, USA) with FastStart™ Universal SYBR® Green Master (04913914001; Roche). The primer sequences are detailed in Supplementary Table S2.

Animals

Eight-week-old female C57BL/6J mice (24–28 g; Vital River Laboratory Animal Technology, Beijing, China) were maintained under SPF conditions with controlled temperature (24 ± 2°C), relative humidity (50% ± 10%), and a 12-h light/dark cycle. All animal experiments, including euthanasia, were conducted in accordance with protocols approved by the Ethics Committee of Qingdao Marine Biomedical Research Institute (E-MBKYY-2022-9-132).

Mouse primary peritoneal macrophage isolation and culture

The procedure for isolating primary macrophages from the peritoneal cavity of mice was carried out following an established method [29]. In brief, 38.5 g BBL™ Thioglycollate Medium Brewer Modified (211716; BD Biosciences, San Jose, USA) was dissolved in 1 L of purified water under continuous stirring, followed by sterilization by autoclaving (121°C, 15 min). The solution was stored at 4°C and used within three months. Each mouse received an intraperitoneal injection of 1 mL of the solution. After 72 h, the mouse was euthanized, and peritoneal macrophages were collected by lavage of the peritoneal cavity with cold PBS. The cells were cultured in DMEM with 10% fetal bovine serum (FBS; Gibco, New York, USA), 1% penicillin and streptomycin.

BLM-induced PF mouse model

Animals were randomly divided into three groups: the control group (NC, $n = 16$), the BLM-induced PF group (BLM, $n = 16$), and the T4015 treatment group (BLM + T4015, $n = 16$). Pulmonary fibrosis was induced on day 0 by a single oropharyngeal instillation of 50 μL BLM (T6116; Topscience) at 5 mg/kg [30] under anesthesia with 2,2,2-tribromoethanol (T48402; Sigma-Aldrich, St Louis, USA). Control mice received an equivalent volume of PBS. Mice in the T4015 group were orally administered T4015 (5 mg/kg in 0.5% carboxymethyl cellulose sodium) once every other day. Throughout the duration of the experiment, body weight and survival were monitored daily. On day 25, the mice were sacrificed, and lung tissues were collected for further analysis and measurement.

Morphological and histological analyses

On day 25, the lungs of mice were collected for histological examination. Lungs were fixed in 4% paraformaldehyde (P1110; Solarbio, Beijing, China), embedded in paraffin, and sectioned. Hematoxylin and Eosin staining (H&E), Masson's trichrome staining, immunohistochemistry and immunofluorescence were performed using standard protocols for histopathological evaluation. Images at magnifications of 40× were analyzed to assess the extent of pulmonary inflammation and fibrosis. Quantification of Masson staining was performed using the open access image processing program ImageJ.

Molecular docking

Molecular docking of T4015 with target proteins, including JAK1 (UniProt ID: P23458), TYK2 (UniProt ID: P29597), EGFR (UniProt ID: Q01279), JAK2 (UniProt ID: Q62120), JAK3 (UniProt ID: Q62137), IRAK1 (UniProt ID: P51617), IRAK4 (UniProt ID: Q9NWZ3), RIPK1 (UniProt ID: Q13546), TAB1 (UniProt ID: Q15750), and ZAP70 (UniProt ID: P43404), was conducted using AutoDock Vina (version 1.1.2). Protein structures were prepared using PyMOL 2.4 by removing water molecules and extraneous ligands and by adding hydrogen atoms. The PDBQT files required for docking simulations were generated with AutoDock Tools 1.5.6. The binding energy (ΔG, kcal/mol) was calculated directly by AutoDock Vina's scoring function. This function is an empirical approximation of the Gibbs free energy of binding and incorporates terms such as van der Waals forces, hydrogen bonding, electrostatic interactions, desolvation, and entropy loss upon binding. Binding energies more negative than −7.0 kcal/mol are considered to indicate strong binding. A more negative value indicates a stronger predicted binding affinity. Docking results were subsequently visualized using PLIP and PyMOL 2.4.

Transcriptome sequencing

Mouse peritoneal macrophages were divided into four groups: vehicle group treated with an equivalent volume of DMSO (NC, $n = 3$), T4015 treatment group treated with 10 μM T4015 for 2 h (T4015, $n = 3$), LPS treatment group stimulated with 100 ng/mL LPS for 30 min (LPS, $n = 3$) [25,26], and T4015-pretreated group treated with both LPS and T4015 (LPS_T4015, $n = 3$). Total RNA was extracted using RNAiso Plus and assessed with an Agilent 5300 Bioanalyzer (Agilent, Santa Clara, USA) and NanoDrop ND-2000 (Thermo Fisher Scientific, Waltham, USA). Sequencing libraries were prepared using the NovaSeq X Plus platform (Illumina, San Diego, USA). PE150 Clean reads were aligned to the mouse reference genome (GRCm39). Differentially expressed genes (DEGs) were identified with DESeq2, and the screening threshold was $|\log_2 FC| \geq 2$ and P adjusted < 0.05. Principal component analysis (PCA) [31], Kyoto Encyclopedia of Genes and Genomes (KEGG)/Gene Ontology (GO) pathway enrichment analysis [32], gene set enrichment analysis (GSEA) [33], Protein-Protein Interaction (PPI) [34], trend analysis [35], and ingenuity pathway analysis (IPA) analysis [36] were performed on DEGs.

Statistical analysis

Data are presented as the mean ± SD. Statistical significance was determined using unpaired Student's t-test or one-way ANOVA. Graphs were generated with GraphPad Prism 9.5 (GraphPad Software, La Jolla, USA). $P < 0.05$ was considered statistically significant.

Results

T4015 suppresses JAK/STAT and NF-κB signaling activation in mouse primary peritoneal macrophages

Based on their binding affinities to STAT and NF-κB-binding elements, we constructed a JAK/STAT and NF-κB dual-target luciferase reporter system SKA-II and established a systematic high-throughput screening procedure as we previously described (Supplementary Figure S1) [25,26]. In this study, we screened 7200 compounds from the TargetMol compound library containing novel, clinical, and marketed bioactive compounds. Filtering by

the inhibitory potencies ($|\log_2 FC| > 1$) and literature search, a bioactive compound, T4015, structure-based design of 4-indolyl-2-phenylaminopyrimidine derivatives, was screened out as a JAK/STAT/NF-κB inhibitor (Figure 1A,B). The physicochemical properties and pharmacokinetics of T4015 were calculated utilizing the SwissADME platform. According to Lipinski's Rule of Five, T4015 has a molecular weight of 532.087, a LogP of 4.816, 8.25 hydrogen bond acceptors, and 2 hydrogen bond donors (Figure 1C). These parameters collectively suggested that T4015 has the potential to exhibit drug-like characteristics.

The JAK/STAT and NF-κB pathways serve as crucial hubs in triggering, amplification, and maintenance of inflammatory responses and immune responses [7]. The effect of T4015 on these pathways was evaluated in mouse primary peritoneal macrophages stimulated with various cytokines and immunologic agonists. T4015 inhibited IL-6-induced STAT3 phosphorylation in a dose-dependent manner, with significant suppression observed at 5 μM (Figure 1D). Furthermore, T4015 was also effective in suppressing the activation of STAT2 induced by IFN-β and the activation of STAT1 induced by IFN-γ (Figure 1E,F). In addition, for the NF-κB signaling pathway activated by LPS and TNFα, phosphorylation of IKK and IκBα degradation was inhibited by T4015 in a concentration-dependent manner (Figure 1G,H). To further assess the inhibitory activity of T4015, we compared its effects with those of Tofacitinib (JAK inhibitor, 10 μM) and BAY-11-7082 (NF-κB inhibitor, 10 μM) in LPS-stimulated macrophages (Supplementary Figure S2A). T4015 (10 μM) markedly reduced STAT3 phosphorylation, with an inhibitory effect comparable to that of the combined positive controls. T4015 modestly increased IκBα protein levels and decreased IKKα/β phosphorylation, although less effectively than BAY-11-7082. To further explore the impact of T4015 on the upstream target protein of the JAK/STAT pathway, the effect of T4015 on IFN-β-stimulated JAK1 and TYK2 phosphorylation was detected. We found that T4015 exerted inhibitory effects on the phosphorylation of both JAK1 and TYK2 (Figure 1I). To further assess its anti-inflammatory properties, the expression of LPS-induced inflammatory cytokines in peritoneal macrophages was measured. T4015 hindered the expression of a multitude of inflammatory cytokines and chemokines induced by LPS, including *Tnf*, *Ifnb*, *Il17a*, *Il6*, and *Cxcl2* (Figure 1J–O and Supplementary Figure S2B–F). These findings suggested that T4015 may exhibit anti-inflammatory effects by inhibiting the JAK/STAT and NF-κB pathways, as well as the expression of their upstream key kinases and downstream target genes in response to immunologic stimulants of the immune system.

Transcriptome sequencing comprehensively demonstrates the anti-inflammatory effects of T4015 in peritoneal macrophages

To evaluate the anti-inflammatory activity of T4015, transcriptome sequencing was performed on peritoneal macrophages treated with DMSO (NC), LPS, T4015, or LPS + T4015 (LPS_T4015) (Figure 2A). The PCA diagram provided a visual representation of each sample grouping and clustering pattern (Supplementary Figure S3A), and the genetic clustering of samples was delineated by the heatmap (Supplementary Figure S3B). These data indicated that T4015 treatment significantly modulated the gene expression profiles induced by LPS. In comparison to the NC group, 547 DEGs were upregulated and 316 DEGs were downregulated in the LPS group, whereas 358 DEGs were upregulated and 545 DEGs were downregulated in the LPS_T4015 group (Figure 2B). The expression of LPS-induced inflammatory genes, including JAK/STAT-related IFIT3 and IFIT1, as well as the cytokines IL1-β and IL-6, was attenuated by T4015 (Figure 2C). KEGG enrichment analysis of upregulated DEGs in the LPS vs NC comparison highlighted pro-inflammatory and immune pathways, including the NF-κB, IL-17, JAK-STAT, and TNF signaling pathways (Figure 2D). Subsequently, DEGs downregulated in the LPS_T4015 vs LPS comparison were enriched in the JAK-STAT, TNF, IL-17, and Toll-like receptor signaling pathways, among other inflammation- and immunity-related pathways (Figure 2E). To elucidate the comprehensive regulatory effects of T4015 treatment on gene function, we performed GSEA enrichment to analyze the gene set between the LPS_T4015 and LPS groups and revealed a downregulation trend in the JAK/STAT-related IL-6 pathway and TNFα signaling via NF-κB (Figure 2F,G). Furthermore, the networks of downregulated upstream regulators in the LPS_T4015 group vs the LPS group were visualized by IPA software, including IRF3 and IFN-γ (Supplementary Figure S3C), as well as NF-κB and IκB-α/β (Supplementary Figure S3D).

As an endotoxin, LPS could stimulate innate immune cells, triggering immune responses and the release of inflammatory mediators [37]. To assess the effects of T4015 on LPS-induced genes, downregulated DEGs in the LPS_T4015 group were compared with upregulated DEGs in the LPS group, revealing that T4015 pretreatment suppressed 214 LPS-induced DEGs (Figure 2H). Central nodes in the network of these DEGs included JAK/STAT-related proteins such as STAT1, IFIT2, and IFIT3, as well as pro-inflammatory cytokines IL-6 and IFN-β (Figure 2I). Then, we performed trend analysis to cluster the gene expression of the NC group, LPS group, and LPS_T4015 group and obtained a statistically significant profile 5 (Supplementary Figure S3E), which encompassed 903 genes upregulated by LPS but downregulated by T4015. KEGG enrichment of DEGs in profile 5 highlighted predominantly inflammation- and immune-related pathways, including JAK/STAT, NF-κB, and Toll-like receptor signaling (Supplementary Figure S3F), while GO analysis indicated significant enrichment of genes involved in immune responses and responses to stimuli (Supplementary Figure S3G).

In summary, these results revealed that T4015 could suppress LPS-induced pro-inflammatory genes in peritoneal macrophages, notably targeting JAK/STAT-, NF-κB-, and Toll-like receptor-related pathways in peritoneal macrophages.

IPA analysis reveals the anti-inflammatory effects of T4015

To systematically elucidate the anti-inflammatory effects and biological mechanisms of T4015, we conducted a comprehensive data integration and comparative analysis between LPS vs NC and LPS_T4015 vs LPS. In the canonical pathway comparison (Figure 3A), T4015 pretreatment significantly dampened the activation of various inflammation-related and oxidative stress-related signaling pathways triggered by LPS, such as NF-κB activation by viruses, iNOS signaling, IL-6 signaling, and IL-17 signaling. Upstream regulator comparison revealed that T4015 pretreatment downregulated numerous upstream regulatory factors associated with inflammation, including upstream factors of the JAK/STAT signaling pathway, such as STAT1, IRF3, and IRF9, as well as upstream

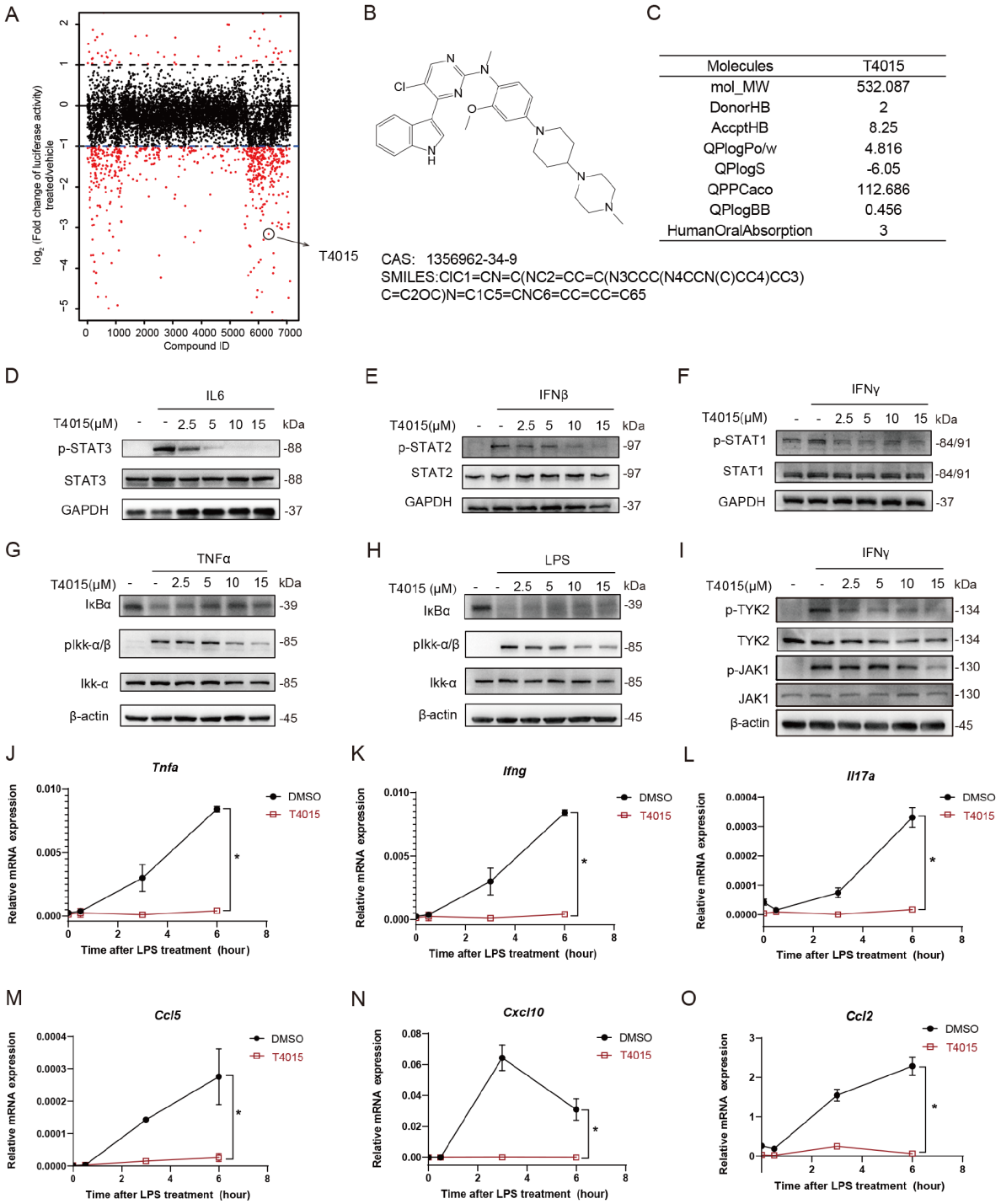

Figure 1. T4015 is identified as an inhibitor of the JAK/STAT and NF-κB signaling pathways (A) Preliminary screening results of 7200 compounds (20 μM) using the JAK/STAT and NF-κB dual-target luciferase reporter system. The preliminary screening results are presented as the log2-fold change in treated/vehicle luciferase activity. (B) Compound structure, molecular weight, and canonical smiles of T4015. (C) The drug properties of T4015 were obtained from SwissADME platform analysis. mol_MW, Molecular weight; DnonorHB, number of H-bond donors; AccptHB, number of H-bond acceptors; QPlogPo/w, Log of octanol/water partition coefficient; QPlogS, Log of aqueous solubility; QPPCaco, Caco-2 permeability; QPlogBB, blood-brain barrier penetration. (D–I) Peritoneal macrophages were pretreated with DMSO or T4015 (2.5, 5, 10, or 15 μM, 2 h), followed by stimulation with IL-6 (5 ng/mL, 10 min) (D), IFN-β (50 ng/mL, 10 min) (E), IFN-γ (50 ng/mL, 10 min) (F,I), TNF-α (20 ng/mL, 10 min) (G), or LPS (100 ng/mL, 30 min) (H). (J–O) Peritoneal macrophages were pretreated with DMSO or T4015 (10 μM, 30 min), followed by LPS stimulation (100 ng/mL) for 0, 0.5, 3, or 6 h. Relative mRNA levels of *Tnf* (J), *Ifng* (K), *Il7a* (L), *Ccl5* (M), *Cxcl10* (N), and *Ccl2* (O) were quantified by RT-PCR. *$P < 0.05$.

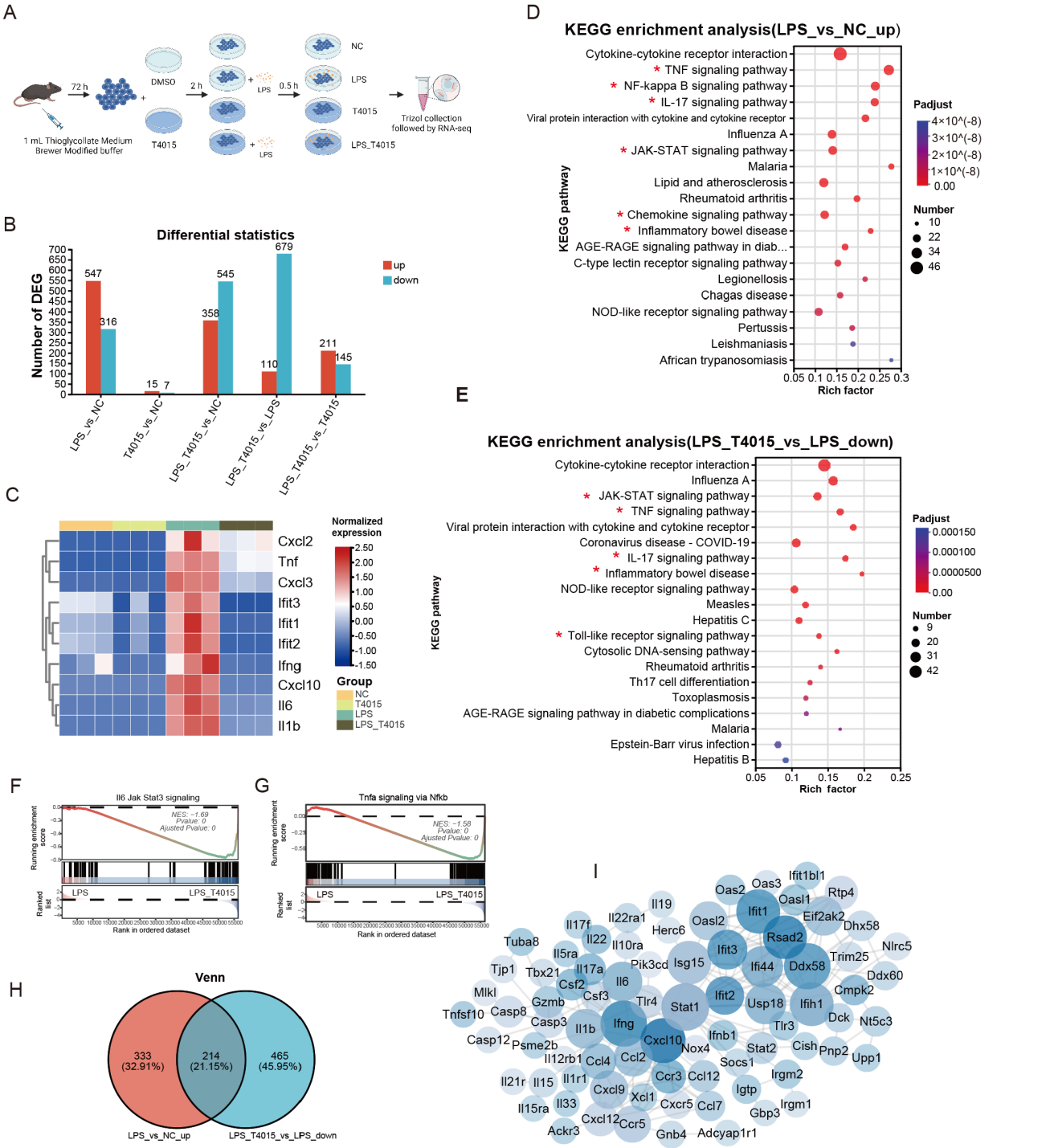

Figure 2. Transcriptome-based analysis of the anti-inflammatory effects of T4015 (A) Schematic workflow of transcriptome sequencing. (B) Pairwise comparison of DEGs among the NC, LPS, T4015, and LPS_T4015 groups. (C) Heatmap of typical pro-inflammatory factors expressed in each group. (D) Top 20 KEGG pathways enriched among DEGs upregulated in LPS vs NC. (E) Top 20 KEGG pathways enriched among DEGs downregulated in LPS_T4015 vs LPS. (F-G) GSEA datasets enriched in downregulated gene clusters of the LPS_T4015 group compared with the LPS group. (H) Venn diagram of upregulated DEGs in the LPS vs NC groups and downregulated DEGs in the LPS_T4015 vs LPS groups. (I) PPI network of 214 shared genes in (H). The size of the circles represents the degree of correlation, blue indicates downregulation, and the shade of color represents the log2-fold change.

factors of the Toll-like signaling pathway, such as TLR3 and TLR4 (Figure 3B). Furthermore, in the biological function comparison analysis (Figure 3C), T4015 pretreatment significantly reduced functions such as the immune response of myeloid cells, pro-inflammatory response, and Th1 immune response. Moreover, in the disease comparison analysis (Figure 3D), T4015 pretreatment

decreased the possibility of terms associated with inflammatory and immune diseases, such as fibrosis of the lung, inflammation of the lung, sepsis, and inflammatory response. The IPA network illustrated the biological interaction network related to the disease terms inflammation of the lung (Figure 3E), interstitial lung disease, and fibrogenesis (Figure 3F). In these networks, the major genes were significantly downregulated by T4015, such as *STAT1*, *IFN-γ*, *IL-6*, and *IL-22* (Figure 3E,F). The IPA data analysis confirmed that T4015 could exert anti-inflammatory effects through the JAK/STAT and NF-κB signaling pathways and suggested its putative applications for the treatment of inflammation-related diseases, especially pulmonary fibrosis and sepsis.

T4015 alleviates BLM-induced pulmonary fibrosis in mice

Pulmonary fibrosis is a diffuse interstitial lung disease characterized by alveolar inflammation in the early stages, which later progresses to excessive proliferation of fibroblasts and extensive extracellular matrix deposition [16,24]. JAK/STAT and NF-κB signaling are extensively involved in the occurrence and progression of pulmonary fibrosis [22,23]. To verify the anti-inflammatory effect of T4015 *in vivo*, we employed a BLM-induced pulmonary fibrosis mouse model to assess its therapeutic potential in inflammatory conditions. T4015 treatment increased the survival rate in pulmonary fibrosis mice and significantly reduced the lung coefficient (Figure 4A–C), which is an indicator measuring the severity of pulmonary pathology. Compared to the BLM group, T4015 did not significantly affect the body weight of mice. Of note, on day 17, several very weak and dying mice died in the BLM group, resulting in a continuous increase in the average body weight of this group (Figure 4D). The pathological features of PF include destruction of alveolar structure, extensive deposition of collagen, infiltration of inflammatory cells, and formation of fibrotic honeycomb lungs [22,23]. Compared with the control group, mice with BLM-induced PF displayed alveolar septal thickening (indicated by arrows) and destruction of the trachea and alveolar structures (indicated by boxes). T4015 treatment effectively alleviated the pathological symptoms and blocked the progression of pulmonary fibrosis (Figure 4E). Treatment with T4015 markedly attenuated collagen deposition in lung tissues, as indicated by the highlighted regions (indicated by boxes) (Figure 4F). Pulmonary fibrosis progression is driven, in part, by inflammatory cytokines and chemokines that promote the differentiation of lung fibroblasts into myofibroblasts [22–24]. T4015 administration significantly reduced the pulmonary expression of *Il6* and *Ccl2* in the lungs of fibrotic mice, as expected (Figure 4G,H). Subsequently, we examined the effects of T4015 on fibrosis-related proteins in lung tissue and discovered that T4015 reduced the expression of COL1, which was associated with collagen formation in the lungs (Figure 4I). To investigate whether the ameliorative effect of T4015 on pulmonary fibrosis involves inhibition of the JAK/STAT and NF-κB pathways *in vivo*, lung tissues from BLM-induced mice were examined by immunohistochemistry and immunofluorescence staining. Immunohistochemical analysis revealed that BLM treatment markedly increased p-STAT3 expression in lung tissues, whereas T4015 administration significantly reduced p-STAT3 levels (Figure 4J). In parallel, immunofluorescence staining demonstrated that T4015 treatment elevated IκB protein expression compared with the BLM group (Figure 4K). These findings indicate that T4015 can inhibit the activation of the JAK/STAT and NF-κB signaling pathways in the lungs of mice, which may contribute to its protective effects against pulmonary fibrosis. Collectively, these results suggested that T4015 treatment mitigated BLM-induced PF and may serve as a promising therapeutic candidate for the condition.

Target fishing and activity exploration of T4015 and its structural analogs

To deeply delve into the putative molecular targets of T4015, we conducted virtual target fishing and molecular docking [38–40]. Leveraging the PharmMapper and GalaxySagittarius databases, we predicted potential targets of T4015 and identified 76 putative targets shared in these two databases, 110 targets specifically in PharmMapper and 424 targets specifically in GalaxySagittarius (Figure 5A). Among them, JAK1, JAK2, JAK3, and TYK2 were key kinases for downstream STAT activation of the JAK/STAT signaling pathways (Supplementary Figure S4A), as well as EGFR, which was reported to activate STAT3 in a JAK1/JAK2-dependent manner [41]. For its inhibition of NF-κB activation induced by TNF and LPS, RIPK1, IRAK1/4, and TAB1 were predicted as the putative drug targets of T4015 (Supplementary Figure S4B). Additionally, ZAP70 could sense extracellular antigens to activate downstream IKK/IκB/NF-κB signaling through the T-cell receptor [42] and was identified as T4015's target in both databases (Figure 5A). Subsequently, we utilized AutoDock Vina 1.1.2 software to molecularly dock these ten targets with T4015, revealing that all were capable of stable binding to T4015 (Figure 5B–H and Supplementary Figure S4C–F). Based on the molecular docking findings, T4015 could bind to pockets of JAK receptor association and phosphotyrosine binding domains (Figure 5C,D and Supplementary Figure S4C,D), which are crucial for its activity. The pyrimidine and indole groups of T4015 could engage in π-π stacking interactions with key kinases, including JAK2, TYK2, IRAK4, and JAK3. Additionally, the methylpiperazine and piperidine moieties of T4015 predominantly facilitated hydrophobic interactions and the formation of salt bridges (Figure 5C–H and Supplementary Figure S4C–F), which further stabilized the complex. In conclusion, the target fishing and molecular docking studies indicated that T4015 has the potential to inhibit the JAK/STAT and NF-κB signaling pathways by directly targeting and suppressing the upstream putative targets JAK1, JAK2, TYK2, JAK3, EGFR, ZAP70, RIPK1, IRAK1/4, and TAB1.

EGFR was predicted to be one of the most putative drug targets of T4015 (Figure 5A,B), and T4015 was structurally derived from the EGFR inhibitor Osimertinib [43]. Therefore, we further collected 15 analogs, including Osimertinib, to investigate the relationship of compound structures and dual JAK/STAT and NF-κB signaling inhibition ability (Figure 5I). Among these 15 analogs, seven compounds were identified as EGFR inhibitors (Supplementary Table S3), four were CDK inhibitors, and others were DYRK, FLT, ALK, or P-GP inhibitors. As shown in Figure 5I, compounds 2 (DYRKi), 8 (EGFRi) and 4 (EGFRi, Osimertinib) did not exhibit inhibitory capacities at either 5 μM or 10 μM, while compound 3 (EGFRi) exhibited inhibitory activities only at a higher dose (10 μM). Meanwhile, compound 1 (ALK/IGFRi) exhibited comparable inhibitory potency as T4015, while others, including EGFRis, CDKis, and other targeting drugs, also exhibited stronger or weaker inhibitory activities compared with T4015. These data suggested that EGFR targeting is not tightly correlated with the inhibitory activities of the compounds for the dual JAK/STAT and NF-κB

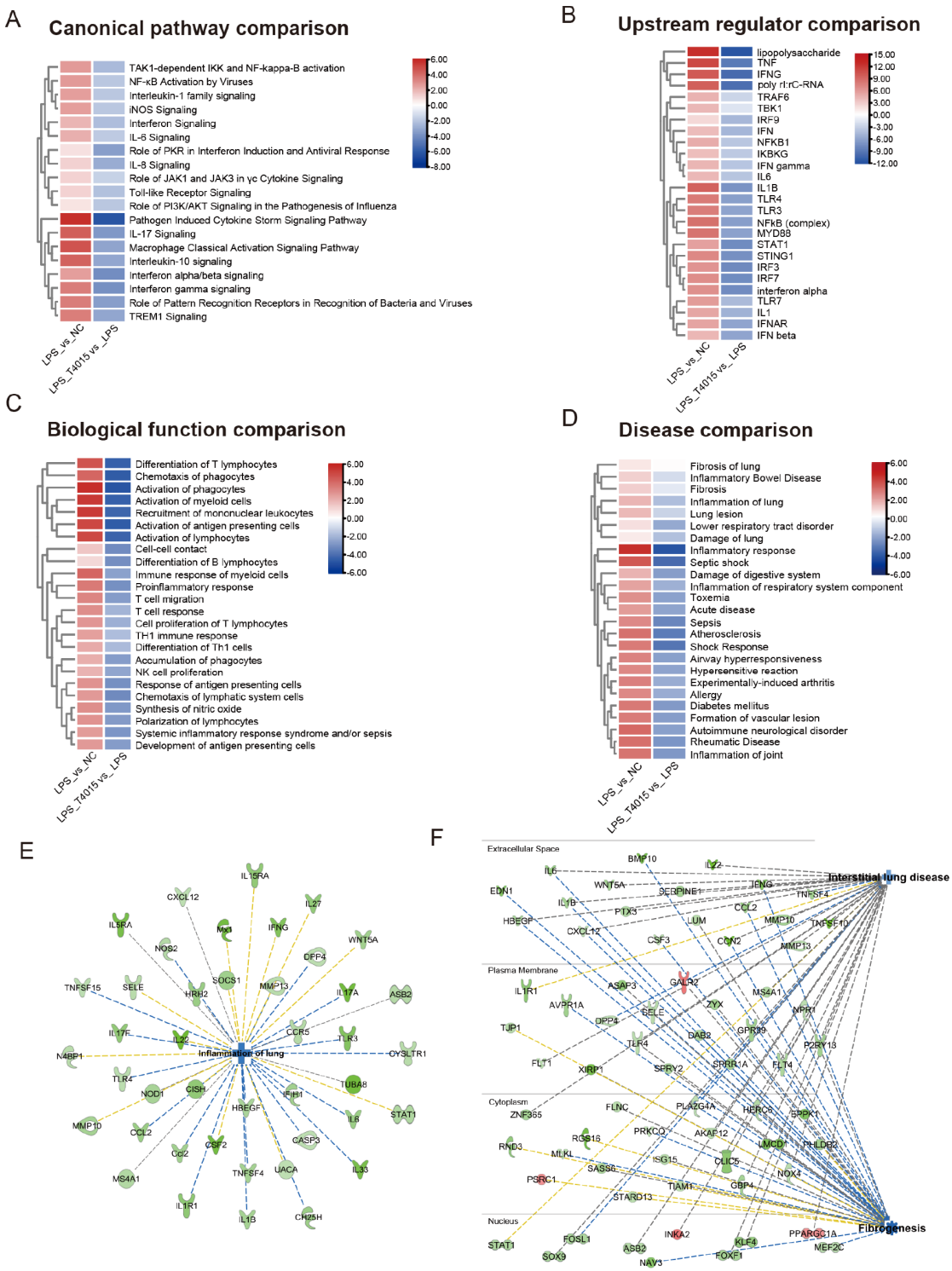

Figure 3. The IPA analysis comparatively assesses the anti-inflammatory effects of T4015 (A-D) Canonical pathway comparison (A), upstream regulator comparison (B), biological function comparison (C), and disease comparison (D) were conducted by comparing significant differences between LPS_T4015 vs LPS and LPS vs NC. Positive z scores indicated predicted activation, whereas negative z scores indicated predicted inhibition in specific terms. (E,F) Disease and function network of the decreased disease terms in LPS_T4015 vs LPS, including inflammation of the lung (E), interstitial lung disease, and fibrogenesis (F). Red represents upregulated genes, green indicates downregulated genes, and the shade of color represents the log2-fold change.

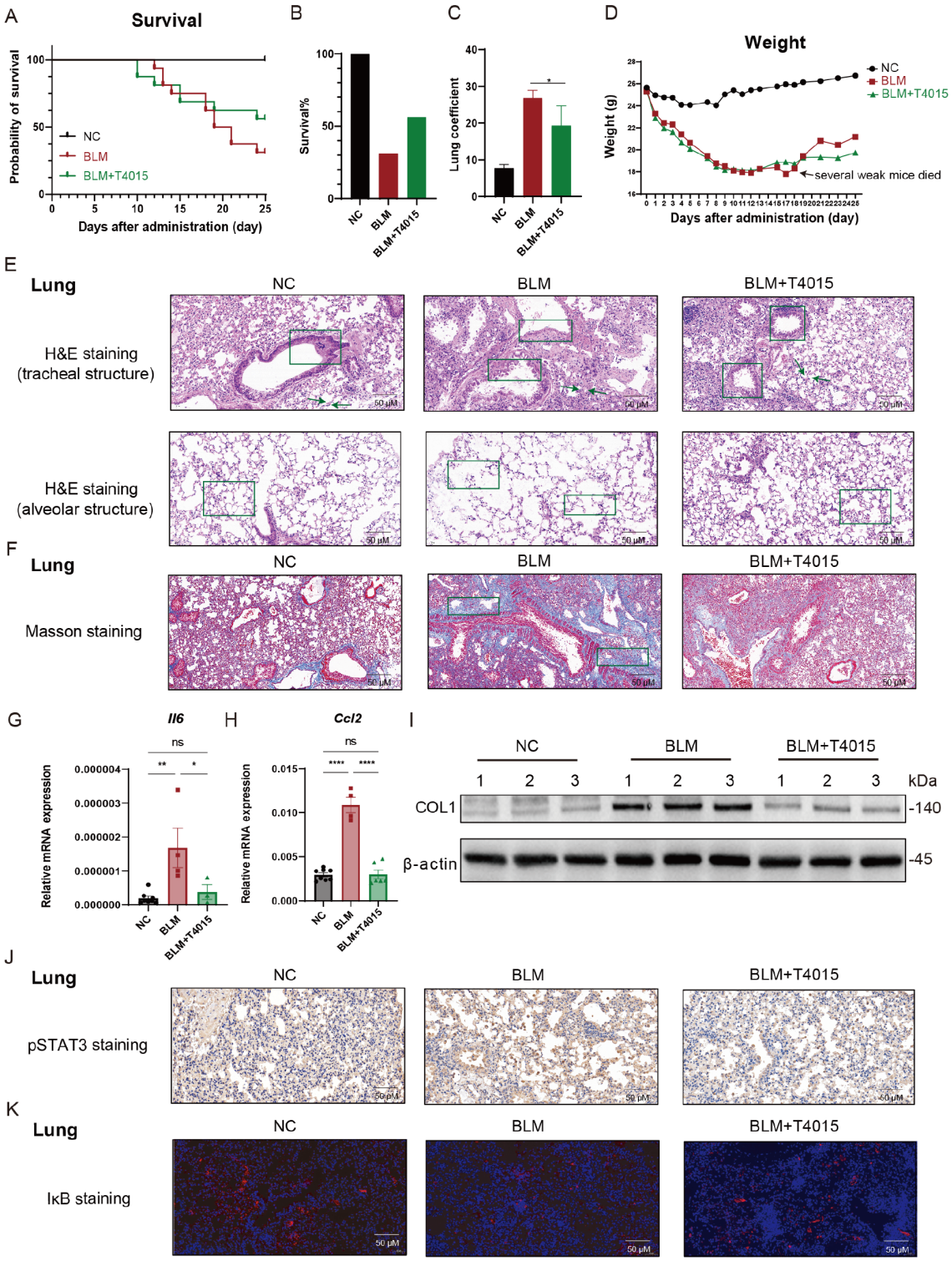

Figure 4. T4015 ameliorates BLM-induced pulmonary fibrosis in mice (A) Daily probability of survival after administration in the NC, BLM, and BLM + T4015 groups. (B,C) Survival rate (B) and lung coefficient (C) of mice in the NC, BLM, and BLM + T4015 groups. (D) Statistical charts of daily body weight. (E,F) H&E staining and Masson staining of lung tissues in the NC, BLM, and BLM + T4015 groups. Scale bar, 50 μm. The boxed area in the upper H&E staining shows the tracheal structure, arrows indicate the thickening of the alveolar septa, and the boxed area in the lower H&E staining shows the alveolar structure (E). The boxed area in the 40× Masson staining represents collagen deposition (F). (G,H) Relative mRNA expression of *Il6* (G) and *Ccl2* (H) in lung tissues assessed by RT-PCR. (I) Western blot analysis of collagen I in lung tissue lysates. (J) Immunohistochemistry of pSTAT3 in mouse lung tissues. Scale bar, 50 μm. (K) Immunofluorescence staining of mouse lung tissues, with red representing IκB and blue representing DAPI. Scale bar, 50 μm. *$P<0.05$, **$P<0.01$, ****$P<0.0001$, and ns means $P>0.05$.

luciferase systems.

Next, we compared the structural similarity and dissimilarity of these analogs and linked them to their inhibitory capacities to the JAK/STAT and NF-κB dual-target reporter system (Figure 5I and Supplementary Figure S5A,B). It was observed that analogs with EGFR inhibitory activity all share a common tail structural feature similar to Osimertinib, and their inhibitory effects on the JAK/STAT and NF-κB pathways are associated with the substituent group on the indole part (highlighted by a green circle). Among these analogs with EGFR inhibitory activity reported, compounds 3, 4, and 8, which lack substituents or have only one methyl substitution, showed no activity (Figure 5I and Supplementary Figure S5A). The analogs without EGFR inhibitory activity all have diverse tails different from Osimertinib (as indicated by a blue circle, in Figure 5J), the majority of which showed significant inhibitory effects. These structural differences could affect the inhibitory capacities of the dual JAK/STAT and NF-κB luciferase systems. Compounds 5, 12, and 14, which contain α,β-unsaturated amide bonds and two hexagonal ring structures connected by an amide bond in the tail structure, had superior inhibitory activity. Modifying the 4-indolyl-2-aminopyrimidine framework demonstrated weak inhibitory activity, such as compound 15 devoid of an amino substitution at pyrimidine (Figure 5I and Supplementary Figure S5B). Furthermore, compound 2, which has a modified indole structure

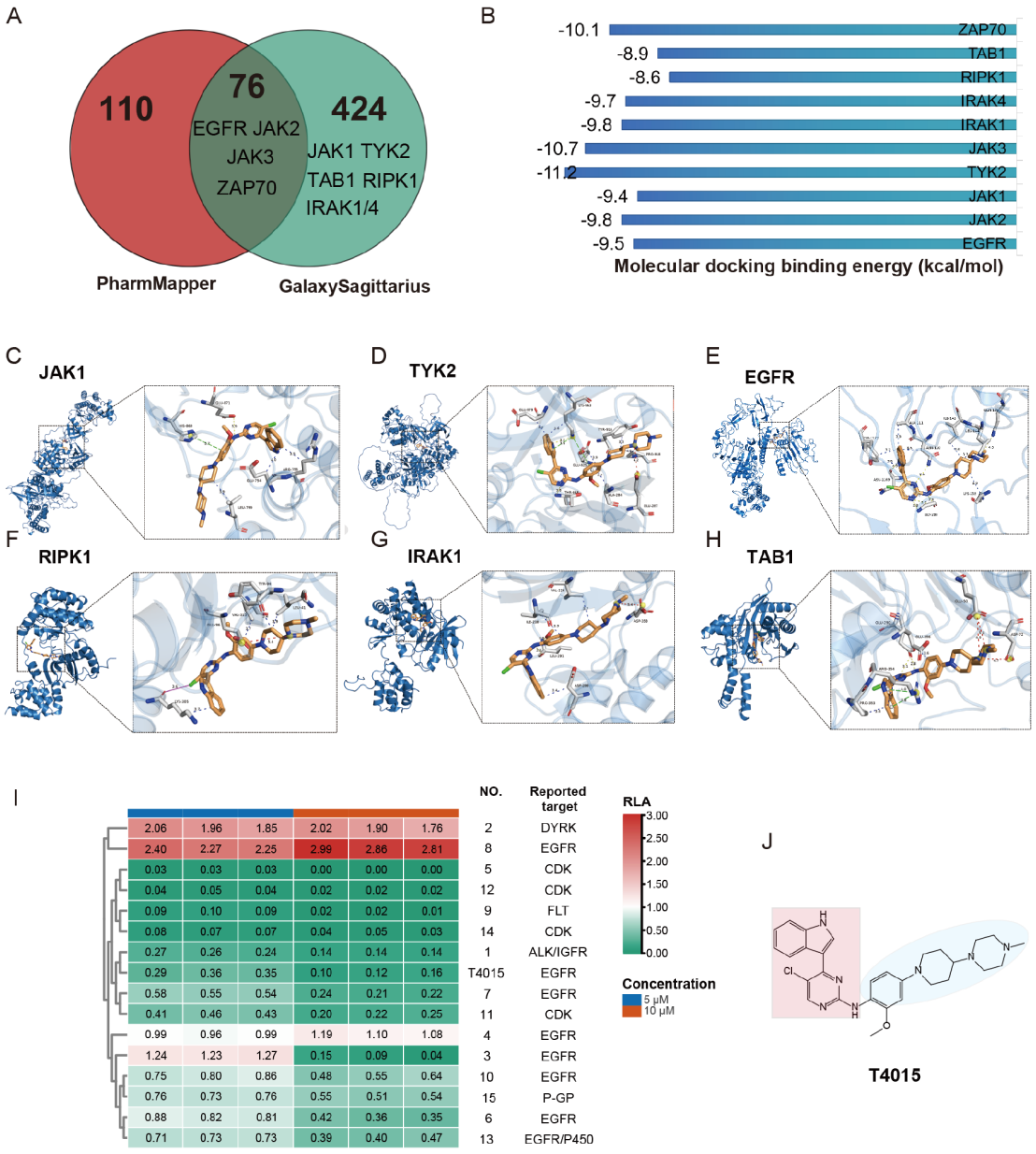

Figure 5. Target fishing and activity exploration of T4015 and its structural analogs (A) Venn diagram of the target fishing results for T4015 using PharmMapper and GalaxySagittarius platforms. (B–H) Molecular docking results of T4015 with proteins JAK1 (C), TYK2 (D), EGFR (E), RIPK1 (F), IRAK1 (G), and TAB1 (H) using AutoDock Vina 1.1.2; binding energies are summarized in (B). (I) Heatmap of the inhibitory activity of T4015 and its analogs at 5 μM and 10 μM concentrations on the JAK/STAT and NF-κB dual-target luciferase reporter system. Interaction types are shown in yellow (hydrogen bonds), blue (hydrophobic), red (salt bridges), green (π-π stacking), and purple (halogen bonds). (J) Chemical structure of T4015.

compared to T4015, exhibited no inhibitory capability (Figure 5I,J and Supplementary Figure S5B). These data suggested that the 4-indolyl-2-aminopyrimidine framework may be responsible for the inhibitory activity of T4015 and its analogs and that the substituents on the nitrogen atom of the indolyl group and the tail substituents of the analogs could be crucial for their anti-JAK/STAT/NF-κB signaling capacities.

Discussion

Inflammation is a critical component of the body's response to injury and infection [20], and its dysregulation is closely linked to the onset and progression of chronic inflammatory and fibrotic diseases. The JAK/STAT and NF-κB signaling pathways serve as central regulators of inflammatory responses and immune activation. Increasing evidence has highlighted the complex crosstalk between these two pathways, including shared upstream regulators, downstream targets, and feedback loops [10,11]. Thus, compounds capable of simultaneously inhibiting both pathways may offer enhanced therapeutic benefits compared to single-pathway inhibitors. In this study, we utilized a high-throughput reporter system to screen out the JAK/STAT and NF-κB dual-target inhibitor T4015, which is based on the structure of the 4-indolyl-2-phenylaminopyrimidine derivative. It could effectively suppress LPS-induced expression of proinflammatory cytokines *in vitro*. Transcriptome analysis revealed that T4015 could downregulate various inflammatory and immune-related signaling pathways, including the JAK-STAT, NF-κB, TNF, IL-17, and Toll-like receptor signaling pathways. Subsequent analysis using IPA software revealed multiple terms related to pulmonary fibrosis and pneumonia, highlighting the potential therapeutic implications of T4015. Furthermore, in the BLM-induced PF mouse model, T4015 significantly decreased the mRNA expression of *Il6* and *Ccl2*, as well as the production of collagen protein COL1 in the lungs. Additionally, it improved the survival rate of mice and diminished the severity of pulmonary fibrosis lesions, demonstrating promising potential for treating pulmonary fibrosis.

At the beginning of inflammation, the chemokine monocyte chemoattractant protein (MCP)-1/CCL2 recruits proinflammatory monocytes expressing CCR2, which subsequently differentiate into macrophages, while T cells are activated and polarize into Th1, Th17, and Treg subsets [44,45]. Macrophages and Th cells serve as primary cellular sources of interleukins that activate NF-κB and JAK-STAT signaling, thereby amplifying the inflammatory response through recruitment of additional immune cells and secretion of proinflammatory cytokines and chemokines [46]. In our biological function comparison analysis (Figure 3C), T4015 was predicted to significantly downregulate immune-related processes, including differentiation of T lymphocytes, natural killer (NK) cell proliferation, and immune of myeloid cells. Furthermore, NK cells and B cells participate in the inflammatory process [47]. NK cells detect infections through their activation receptors NKG2D and NKp46, releasing lytic granules (perforin, granzymes) or engaging in TNF-related apoptosis [48].

BLM, an antineoplastic agent, is utilized for the treatment of various cancers and lymphomas [49]. However, it possesses certain toxicities, with the most severe side effect being pulmonary toxicity, leading to the remodeling of lung structure and the loss of lung function and causing adverse effects such as pulmonary fibrosis [49,50]. Due to its simplicity and reproducibility in inducing pulmonary fibrosis, as well as its similarity to the pathological process of human pulmonary fibrosis, BLM is currently an ideal model for studying the drug effects on pulmonary fibrosis [51]. Notably, in BLM-induced fibrosis mouse models, JAK1 is overexpressed in lung tissues and localized in inflammatory cells and epithelial cells [52]. When validating the inhibitory effect of T4015 on the JAK/STAT signaling pathway *in vitro*, it was found that T4015 could inhibit IFN-γ-induced phosphorylation of JAK1 and TYK2. In addition, JAK1 and TYK2 were also predicted as targets of T4015 in target fishing. In addition, transcriptome sequencing analysis, including KEGG and GO enrichment analysis, consistently confirmed that T4015 could be responsible for the downregulation of the JAK/STAT signaling pathway, implying a possible mechanism of T4015 in treating pulmonary fibrosis.

As previously reported [43], T4015 is a product of the structural modification of Osimertinib, featuring the 4-indolyl-2-phenylaminopyrimidine framework. As we reported, T4015 could exert anti-inflammatory effects by inhibiting the JAK/STAT and NF-κB signaling pathways and showed a promising therapeutic effect in a BLM-induced pulmonary fibrosis mouse model. Through target fishing and molecular docking, we discovered that T4015 may suppress the JAK/STAT/NF-κB pathway by targeting upstream kinase proteins such as JAK1, JAK2, TYK2, RIPK1, and TAB1 (Figure 5A–H). The molecular docking results revealed that the binding site of T4015 with TYK2 includes residues GLU-979, THR-668, LYS963, GLU925, TYR916, ALA242, PRO918 and GLU-287 (Figure 5D). The indole group of T4015 is involved in the formation of hydrogen bonds and π-π stacking interactions, while the piperidine group at the tail contributes significantly to the hydrophobic interactions. Residues involved in the binding site of T4015 with ZAP70 are PHE-348, ASN-347, LYS-499, TRP-500, and ALA-494. Both the indole and piperidine moieties of T4015 participate in the formation of π-π stacking interactions (Supplementary Figure S4E). The activity testing and structural analysis of T4015 and its analogs in the JAK/STAT/NF-κB pathway may suggest the capacity of the 4-indolyl-2-aminopyrimidine framework and the tail structure for the inhibitory capacities of dual JAK/STAT and NF-κB signaling (Figure 5I–J and Supplementary Figure S5A–B). This observation may point toward a feasible direction for structural modifications of anti-inflammatory and antifibrotic candidate drugs targeting the JAK/STAT and NF-κB pathways based on this scaffold. However, to further confirm the direct targets and validate our conclusions, target fishing of labeling compounds and structural modifications are still needed.

Nevertheless, several limitations should be acknowledged. While our data demonstrate that T4015 concurrently inhibits JAK/STAT and NF-κB signaling and ameliorates pulmonary fibrosis, the exact causal relationship between pathway inhibition and therapeutic efficacy warrants further validation. Future studies using genetic approaches (*e.g.*, pathway-specific agonists or conditional knockout models) will be essential to definitively establish whether the anti-fibrotic effects are directly mediated through dual-pathway inhibition. Second, the current *in vivo* study employed a single dose of T4015. This choice was guided by preliminary tolerability testing and pharmacological feasibility; however, comprehensive dose–response evaluations will be essential in future work to better define the therapeutic window. In addition, we note that no direct positive control inhibitor was included in the current experiments, which limits direct comparison with existing therapies. Future studies will

incorporate benchmark JAK/STAT or NF-κB inhibitors to further contextualize T4015's activity.

These observations suggest that the 4-indolyl-2-aminopyrimidine scaffold, particularly when coupled with hydrophobic tail modifications, could serve as a promising template for designing dual inhibitors of the JAK/STAT and NF-κB pathways. Nevertheless, further studies, including labeled compound-based target validation and structure–activity relationship (SAR) optimization, are warranted to fully elucidate the molecular targets and improve the therapeutic potential of T4015 and its analogs.

Supplementary Data

Supplementary data are available at *Acta Biochimica et Biophysica Sinica* online.

Data Availability

Sequencing raw data have been deposited in NCBI GEO (GSE283898).

Funding

This work was supported by the grants from the National Natural Science Foundation of China (No. 32470764), the National Natural Science Foundation of China for Young Scholar Project (No. 82404586), the Natural Science Foundation of Qingdao Municipality Project (No. 2444zrjj101jch), and Shandong Province Traditional Chinese Medicine Science and Technology Project (No. 2020M108).

Conflict of Interest

The authors declare that they have no conflict of interest.

References

1. Thannickal VJ, Toews GB, White ES, Lynch III JP, Martinez FJ. Mechanisms of pulmonary fibrosis. *Annu Rev Med* 2004, 55: 395–417
2. Rockey DC, Bell PD, Hill JA. Fibrosis–a common pathway to organ injury and failure. *N Engl J Med* 2015, 372: 1138–1149
3. Spagnolo P, Maher TM, Richeldi L. Idiopathic pulmonary fibrosis: recent advances on pharmacological therapy. *Pharmacol Ther* 2015, 152: 18–27
4. Lederer DJ, Martinez FJ. Idiopathic pulmonary fibrosis. *N Engl J Med* 2018, 378: 1811–1823
5. Martinez FJ, Collard HR, Pardo A, Raghu G, Richeldi L, Selman M, Swigris JJ, *et al.* Idiopathic pulmonary fibrosis. *Nat Rev Dis Primers* 2017, 3: 17074
6. Li X, Wang Y, Liang J, Bi Z, Ruan H, Cui Y, Ma L, *et al.* Bergenin attenuates bleomycin-induced pulmonary fibrosis in mice via inhibiting TGF-β1 signaling pathway. *PhytoTher Res* 2021, 35: 5808–5822
7. Liu J, Wang F, Luo F. The role of JAK/STAT pathway in fibrotic diseases: molecular and cellular mechanisms. *Biomolecules* 2023, 13: 119
8. Tefferi A, Lasho TL, Schwager SM, Steensma DP, Mesa RA, Li CY, Wadleigh M, *et al.* The JAK2^{V617F} tyrosine kinase mutation in myelofibrosis with myeloid metaplasia: lineage specificity and clinical correlates. *Br J Haematol* 2005, 131: 320–328
9. Shuai K, Liu B. Regulation of JAK-STAT signalling in the immune system. *Nat Rev Immunol* 2003, 3: 900–911
10. Pedroza M, Le TT, Lewis K, Karmouty-Quintana H, To S, George AT, Blackburn MR, *et al.* STAT-3 contributes to pulmonary fibrosis through epithelial injury and fibroblast-myofibroblast differentiation. *FASEB Journal* 2016, 30: 129–140
11. Pechkovsky DV, Prêle CM, Wong J, Hogaboam CM, McAnulty RJ, Laurent GJ, Zhang SSM, *et al.* STAT3-mediated signaling dysregulates lung fibroblast-myofibroblast activation and differentiation in UIP/IPF. *Am J Pathol* 2012, 180: 1398–1412
12. Wright JG, Christman JW. The role of nuclear factor kappa B in the pathogenesis of pulmonary diseases: implications for therapy. *Am J Respir Med* 2003, 2: 211–219
13. Vallabhapurapu S, Karin M. Regulation and function of NF-κB transcription factors in the immune system. *Annu Rev Immunol* 2009, 27: 693–733
14. Lawrence T. The nuclear factor NF-κB pathway in inflammation. *Cold Spring Harb Perspect Biol* 2009, 1: a001651
15. Guo Q, Jin Y, Chen X, Ye X, Shen X, Lin M, Zeng C, *et al.* NF-κB in biology and targeted therapy: new insights and translational implications. *Sig Transduct Target Ther* 2024, 9: 53
16. Peng L, Wen L, Shi QF, Gao F, Huang B, Meng J, Hu CP, *et al.* Scutellarin ameliorates pulmonary fibrosis through inhibiting NF-κB/NLRP3-mediated epithelial–mesenchymal transition and inflammation. *Cell Death Dis* 2020, 11: 978
17. Dong J, Ma Q. *In vivo* activation and pro-fibrotic function of NF-κB in fibroblastic cells during pulmonary inflammation and fibrosis induced by carbon nanotubes. *Front Pharmacol* 2019, 10: 1140
18. Gross CM, Kellner M, Wang T, Lu Q, Sun X, Zemskov EA, Noonepalle S, *et al.* LPS-induced acute lung injury involves NF-κB-mediated downregulation of SOX18. *Am J Respir Cell Mol Biol* 2018, 58: 614–624
19. Cui Y, Jiang L, Yu R, Shao Y, Mei L, Tao Y. β-carboline alkaloids attenuate bleomycin induced pulmonary fibrosis in mice through inhibiting NF-κB/p65 phosphorylation and epithelial-mesenchymal transition. *J EthnoPharmacol* 2019, 243: 112096
20. Philips RL, Wang Y, Cheon HJ, Kanno Y, Gadina M, Sartorelli V, Horvath CM, *et al.* The JAK-STAT pathway at 30: much learned, much more to do. *Cell* 2022, 185: 3857–3876
21. Yu H, Lin L, Zhang Z, Zhang H, Hu H. Targeting NF-κB pathway for the therapy of diseases: mechanism and clinical study. *Sig Transduct Target Ther* 2020, 5: 209
22. Grivennikov SI, Karin M. Dangerous liaisons: STAT3 and NF-κB collaboration and crosstalk in cancer. *Cytokine Growth Factor Rev* 2010, 21: 11–19
23. Mitchell S, Mercado EL, Adelaja A, Ho JQ, Cheng QJ, Ghosh G, Hoffmann A. An NFκB activity calculator to delineate signaling crosstalk: type I and II interferons enhance NFκB via distinct mechanisms. *Front Immunol* 2019, 10: 1425
24. Ivanenkov YA, Balakin KV, Lavrovsky Y. Small molecule inhibitors of NF-κB and JAK/STAT signal transduction pathways as promising anti-inflammatory therapeutics. *MRMC* 2011, 11: 55–78
25. Li M, Yan Y, Zhang X, Zhang Y, Xu X, Zhang L, Lu L, *et al.* Scaffold compound L971 exhibits anti-inflammatory activities through inhibition of JAK/STAT and NFκB signalling pathways. *J Cell Mol Medi* 2021, 25: 6333–6347
26. Xu J, Zhang X, Zhou M, Lu P, Xu Y, Wu L, Zhang Q, *et al.* Bioactive compound C498-0670 alleviates LPS-induced sepsis via JAK/STAT and NFκB signaling pathways. *Front Immunol* 2023, 14: 1132265
27. Reddig A, Voss L, Guttek K, Roggenbuck D, Feist E, Reinhold D. Impact of different JAK inhibitors and methotrexate on lymphocyte proliferation and DNA damage. *J Clin Med* 2021, 10: 1431
28. Strickson S, Campbell DG, Emmerich CH, Knebel A, Plater L, Ritorto MS, Shpiro N, *et al.* The anti-inflammatory drug BAY 11-7082 suppresses the MyD88-dependent signalling network by targeting the ubiquitin system. *Biochem J* 2013, 451: 427–437
29. Zhao C, Pavicic PG, Datta S, Sun D, Novotny M, Hamilton TA. Cellular stress amplifies TLR3/4-Induced CXCL1/2 gene transcription in mononuclear phagocytes via RIPK1. *J Immunol* 2014, 193: 879–888

30. Gul A, Yang F, Xie C, Du W, Mohammadtursun N, Wang B, Le J, *et al.* Pulmonary fibrosis model of mice induced by different administration methods of bleomycin. *BMC Pulm Med* 2023, 23: 91
31. Han C, Shi C, Liu L, Han J, Yang Q, Wang Y, Li X, *et al.* Majorbio cloud 2024: update single-cell and multiomics workflows. *iMeta* 2024, 3: e217
32. Mu H, Chen J, Huang W, Huang G, Deng M, Hong S, Ai P, *et al.* OmicShare tools: a zero-code interactive online platform for biological data analysis and visualization. *iMeta* 2024, 3: e228
33. Madhvi A, Mishra H, Chegou NN, Tromp G, Van Heerden CJ, Pietersen RD, Leisching G, *et al.* Distinct host-immune response toward species related intracellular mycobacterial killing: a transcriptomic study. *Virulence* 2020, 11: 170–182
34. Szklarczyk D, Kirsch R, Koutrouli M, Nastou K, Mehryary F, Hachilif R, Gable AL, *et al.* The STRING database in 2023: protein-protein association networks and functional enrichment analyses for any sequenced genome of interest. *Nucleic Acids Res* 2023, 51: D638–D646
35. Ernst J, Bar-Joseph Z. STEM: a tool for the analysis of short time series gene expression data. *BMC BioInf* 2006, 7: 191
36. Krämer A, Green J, Pollard J, Tugendreich S. Causal analysis approaches in Ingenuity pathway analysis. *Bioinformatics* 2014, 30: 523–530
37. Noailles A, Maneu V, Campello L, Lax P, Cuenca N. Systemic inflammation induced by lipopolysaccharide aggravates inherited retinal dystrophy. *Cell Death Dis* 2018, 9: 350
38. Trott O, Olson AJ. AutoDock vina: improving the speed and accuracy of docking with a new scoring function, efficient optimization, and multithreading. *J Comput Chem* 2010, 31: 455–461
39. Yang J, Kwon S, Bae SH, Park KM, Yoon C, Lee JH, Seok C. Galaxysagittarius: structure- and similarity-based prediction of protein targets for druglike compounds. *J Chem Inf Model* 2020, 60: 3246–3254
40. Wang X, Pan C, Gong J, Liu X, Li H. Enhancing the enrichment of pharmacophore-based target prediction for the polypharmacological profiles of drugs. *J Chem Inf Model* 2016, 56: 1175–1183
41. Wang Y, van Boxel-Dezaire AH, Cheon H, Yang J, Stark GR. STAT3 activation in response to IL-6 is prolonged by the binding of IL-6 receptor to EGF receptor. *Proc Natl Acad Sci USA* 2013, 110: 16975–16980
42. Swamy M. ZAP70 holds the key to kinetic proofreading for TCR ligand discrimination. *Nat Immunol* 2022, 23: 1293–1294
43. Chen H, Lai M, Zhang T, Chen Y, Tong L, Zhu S, Zhou Y, *et al.* Conformational constrained 4-(1-sulfonyl-3-indol)yl-2-phenylaminopyrimidine derivatives as new fourth-generation epidermal growth factor receptor inhibitors targeting T790M/C797S mutations. *J Med Chem* 2022, 65: 6840–6858
44. Dewald O, Zymek P, Winkelmann K, Koerting A, Ren G, Abou-Khamis T, Michael LH, *et al.* CCL2/Monocyte chemoattractant protein-1 regulates inflammatory responses critical to healing myocardial infarcts. *Circ Res* 2005, 96: 881–889
45. Zhao H, Wu L, Yan G, Chen Y, Zhou M, Wu Y, Li Y. Inflammation and tumor progression: signaling pathways and targeted intervention. *Sig Transduct Target Ther* 2021, 6: 263
46. Zabetakis I, Lordan R, Norton C, Tsoupras A. COVID-19: the inflammation link and the role of nutrition in potential mitigation. *Nutrients* 2020, 12: 1466
47. Strandmark J, Steinfelder S, Berek C, Kühl AA, Rausch S, Hartmann S. Eosinophils are required to suppress Th2 responses in Peyer's patches during intestinal infection by nematodes. *Mucosal Immunol* 2017, 10: 661–672
48. Tosello-Trampont A, Surette FA, Ewald SE, Hahn YS. Immunoregulatory role of NK cells in tissue inflammation and regeneration. *Front Immunol* 2017, 8: 301
49. Moeller A, Ask K, Warburton D, Gauldie J, Kolb M. The bleomycin animal model: a useful tool to investigate treatment options for idiopathic pulmonary fibrosis? *Int J Biochem Cell Biol* 2008, 40: 362–382
50. Adamson IY. Pulmonary toxicity of bleomycin. *Environ Health Perspect* 1976, 16: 119
51. Moeller A, Rodriguez-Lecompte JC, Wang L, Gauldie J, Kolb M. Models of pulmonary fibrosis. *Drug Discov Today* 2006, 3: 243–249
52. Montero P, Milara J, Roger I, Cortijo J. Role of JAK/STAT in interstitial lung diseases; molecular and cellular mechanisms. *Int J Mol Sci* 2021, 22: 6211